Spectroscopy of weakly deformed bands in ^{87}Zr: First observation of the shears mechanism in a Zr isotope

P. Banerjee,[1] S. Ganguly,[2] M. K. Pradhan,[1,*] Md. Moin Shaikh,[1,†] H. P. Sharma,[3] S. Chakraborty,[3] R. Palit,[4] R. G. Pillay,[4] V. Nanal,[4] S. Saha,[4,‡] and J. Sethi[4,§]

[1]*Saha Institute of Nuclear Physics, Sector 1, Block AF, Bidhan Nagar, Kolkata 700064, India*

[2]*Department of Physics, Bethune College, Kolkata 700006, India*

[3]*Benaras Hindu University, Varanasi 221005, India*

[4]*Tata Institute of Fundamental Research, Mumbai 400005, India*

(Received 18 April 2018; published 24 September 2018)

Excited states of ^{87}Zr, populated in the reaction ^{60}Ni(^{31}P, $3pn$) at a beam energy of 112.5 MeV, have been studied. Experimental information on two negative-parity bands has been significantly upgraded with the addition of new γ rays and levels. Small values of the reduced transition probability $B(E2)$ and a general absence of a measurable Doppler shift in the transitions suggest that the states are weakly deformed. Several positive-parity levels have been grouped into two bands based on their observed properties. Spin parities have been proposed for a majority of the states belonging to the different bands. Lifetimes have been measured for the eight states belonging to the two positive-parity bands from Doppler shift attenuation data, including an upper limit for the highest energy state. The behavior of the deduced $B(M1)$ and $B(E2)$ values as a function of level spin supports the interpretation of one of these bands within the framework of the shears mechanism. A study of these reduced transition probabilities in the light of the semiclassical model of the shears mechanism, proposed by Macchiavelli and co-workers, confirms this interpretation. The effective gyromagnetic ratio and the interaction strength between the two blades of the shears have been estimated from this study.

DOI: 10.1103/PhysRevC.98.034320

I. INTRODUCTION

Nuclei in the mass region $A = 80$–90 possess diverse structural features such as rapid variation in shape, superdeformation, and short sequences of weakly deformed dipole bands. These nuclei display dramatic transitions in shape from the strongly deformed structures at $N \approx 40$ to the near-spherical ones close to the $N = 50$ shell closure, depending on the occupation of specific orbitals near the Fermi surface. The Zr isotopes ($Z = 40$), for example, show a remarkable change in structure from the highly deformed ^{80}Zr with a quadrupole deformation of $\beta_2 \approx 0.4$ [1] to the ideal spherical nucleus ^{90}Zr [2] through the ^{84,86}Zr isotopes that lie in the transitional region where the structures are neither strongly collective nor significantly spherical. In addition, high-spin superdeformed (SD) bands have been reported in ^{81,82,83}Sr [3–6], ^{82}Y [7], and ^{83,84,86}Zr [8–10]. The observation of these superdeformed bands with $\beta_2 \approx 0.55$ indicates the presence of a large SD shell gap at this deformation for $Z = 38$–40. A great deal of experimental effort in the past has been devoted to the study of the evolution of the nuclear structure with change in neutron number and of the superdeformed structures in this mass region.

The structure of a majority of the $A = 80$–90 nuclei with neutron number close to $N = 50$ is dominated by spherical states. However, there are several nuclei in the neutron midshell region that are weakly deformed and posses short sequences of levels that are connected by strong $M1$ transitions. These bands were first reported in ^{82,84}Rb [11,12] and were found to display properties that resemble those of the magnetic rotors identified in other mass regions such as $A = 110$, 140, and 190. Subsequently, similar bands have been reported in ^{79}Br [13], ^{83}Rb [14,15], and ^{85}Sr [16]. In addition, three-quasiparticle bands have been observed in ^{81,83}Kr [17,18] that display a sharp decrease of the intraband $M1$ transition strengths with increasing frequency. Theoretically, the phenomenon is described within the framework of the tilted-axis cranking model [19] where the rotational axis is oriented away from the principal axes but lies in one of the principal planes.

The nucleus ^{87}Zr, an isotone of ^{83}Kr, ^{84}Rb, and ^{85}Sr with $N = 47$, has been previously studied up to a maximum spin of $(47/2^-)$ from the reaction ^{59}Co(^{32}S, $3pn$) at $E = 118$ MeV using an array of seven Compton-suppressed HPGe detectors [20]. In addition to this, lifetimes of some of the low-spin states have been reported from Doppler shift attenuation (DSA) measurements reflecting weak collectivity [21,22]. However, there is no reported evidence in favor of the

*Present address: Department of Physics, Belda College, Medinipur 721424, India.

†Present address: Inter-University Accelerator Center, New Delhi 110067, India.

‡Present address: GSI Helmholtzzentrum für Schwerionenforschung, Darmstadt, Hesse, Germany.

§Present address: Department of Chemistry and Biochemistry, University of Maryland, College Park, Maryland 20742, USA.

existence of the phenomenon of magnetic rotation in ^{87}Zr so far, although such dipole bands have been observed in most of the neighboring $N = 47$ isotones as noted above. Indeed, magnetic rotation bands have not been reported in any Zr isotopes to date. The present work is an attempt to look for the possible existence of such structures in ^{87}Zr from a detailed investigation of level lifetimes and other nuclear properties.

II. EXPERIMENTAL DETAILS

Excited states of ^{87}Zr were populated in the reaction ^{60}Ni(^{31}P, $3pn$) at a beam energy of 112.5 MeV using the BARC-TIFR Pelletron LINAC facility at the Tata Institute of Fundamental Research, Mumbai, India. The target consisted of 270 μg/cm^2 isotopically enriched (>95%) ^{60}Ni deposited on a 9.3 mg/cm^2 gold backing. Three- and higher-fold coincidence events (equivalent to about 4×10^{10} two- and higher-fold events) were recorded using the Indian National Gamma Array (INGA) comprising nineteen Compton-suppressed Clover detectors. Four of these detectors were positioned at 90° and three detectors at each of the angles 40°, 65°, 115°, 140°, and 157° with respect to the beam direction.

The γ-ray coincidence events were recorded in a fast digital data acquisition system based on Pixie-16 modules of XIA LLC [23]. The data were sorted to generate symmetric $\gamma\gamma$ matrices and $\gamma\gamma\gamma$ cubes which were subsequently analyzed using the software package RADWARE [24]. Gated γ-ray spectra with a dispersion of 0.5 keV per channel were also generated using the computer code INGASORT [25] from 4096×4096 matrices, obtained from the sorting of the gain-matched raw data. Spectra for lifetime analyses using the DSA technique were generated from matrices formed from coincidences between the extreme backward angle (157°) detector events with those in the remaining detectors. The directional correlation of oriented nuclei (DCO) ratios ($R_{\rm DCO}$) for assignment of γ-ray multipolarity were determined from a matrix with events recorded at 90° along one axis and those at 157° along the other. The γ-ray coincidence relationships, required for building the level scheme, were determined from the symmetric $\gamma\gamma$ matrices and $\gamma\gamma\gamma$ cubes using INGASORT and RADWARE, respectively.

Angular correlation information was extracted from coincidence events recorded at 90° and 157° with respect to the beam axis from which the directional correlation intensity ratios ($R_{\rm DCO}$) were extracted. These $R_{\rm DCO}$ ratios were then compared with the calculated values that were obtained using the software package ANGCOR [26] for assignment of level spin I and inferring the γ-ray multipole mixing ratios δ. Gates on stretched $E2$ transitions yield $R_{\rm DCO}$ values close to unity for quadrupole γ rays, although nonstretched pure dipole transitions between states with $\Delta I = 0$ are also known to yield similar $R_{\rm DCO}$ values. For $\Delta I = 1$ γ rays, gates on $E2$ transitions yield DCO ratios ranging from 0 to 2, depending on the value of the $E2/M1$ mixing ratio of the γ ray. For small $\delta_{E2/M1}$ values, the DCO ratios for the $\Delta I = 1$ γ rays are close to 0.5.

The lifetimes of the excited states were extracted from the DSA data using the analysis package LINESHAPE [27]. Details of the procedure adopted for the analyses are discussed subsequently in this text in Sec. III B. The relative intensities of the transitions were determined from gated spectra generated from the symmetric matrices.

III. RESULTS

Experimental results on ^{87}Zr have been previously reported in Refs. [20–22]. Arnell *et al.* [21] reported states up to 4533 keV with $J^\pi \leqslant 27/2^+$ (tentatively up to 5077 keV) from α-induced reactions on ^{84,86}Sr targets. Half-lives of several states using both electronic timing and Doppler shift attenuation techniques were reported in this work. Warburton *et al.* [22] subsequently studied the lifetimes of a few low-energy states in ^{87}Zr using the recoil distance method (RDM) from the Ge (natural) + ^{18}O reaction. The most recent experimental results on ^{87}Zr were reported almost twenty years ago when positive-parity states up to spin $(37/2^+)$ and negative-parity states up to $(43/2^-)$ were reported for the first time [20].

The level scheme of ^{87}Zr deduced from the present work is shown in Fig. 1. The γ-ray relative intensities, indicated by the widths of the arrows (transitions) in the figure, are also given in Tables I–V of the Supplemental Material [28]. It is noted that the γ-ray energies inferred from the present work are consistently larger than those reported in Ref. [20] by up to a keV or more. This leads to level energies, especially in the high-energy regions of the bands, that are considerably more than the values reported in Ref. [20]. However, the present γ-ray and level energies are consistent with those reported in Refs. [21,22].

The levels are grouped into bands 1 to 4 as shown in Fig. 1. Bands 1 and 2 are negative-parity sequences presumably built upon the 2469.4 and 2075.2 keV states and extend up to spins $(37/2^-)$ and $(43/2^-)$, respectively. Bands 3 and 4 are positive-parity bands. While band 3 is built on the 2896.5 keV state with spin $21/2^+$, band 4 is built on the $31/2^+$ state with an excitation energy of 5808.4 keV. Bands 1, 2, and 3 decay down to the low-energy part of the level scheme (that feed into the $9/2^+$ ground state) predominantly through the 416.7, 692.6, and 1004.7 keV γ rays. Several new transitions have been assigned to the level scheme, especially to bands 1 and 2. New transitions and levels observed in this work are marked with asterisks in Fig. 1. Gated spectra in support of the placement of the transitions in the level scheme are shown in Figs. 2, 3, and 6.

A. Bands 1 and 2

New in-band transitions with energies 416.0, 539.1, and 1427.3 keV have been assigned to band 1. The last two transitions lead to an extension of the band with new states at 7385.4 and 8273.7 keV while the 416.0 keV γ ray gives rise to the new level at 3785.9 keV. Similarly, in-band transitions with energies 399.3, 521.4, 662.0, 703.8, and 1352.1 keV, not reported previously, have been observed to connect states belonging to band 2. Three of these states with excitation energies 4592.3, 5296.1, and 6936.8 keV are new additions to band 2. Bands 1 and 2 are connected by several linking transitions of which the ones with energies 718.3, 740.0, 1055.0, 1239.5, and 1399.2 keV have been observed for the

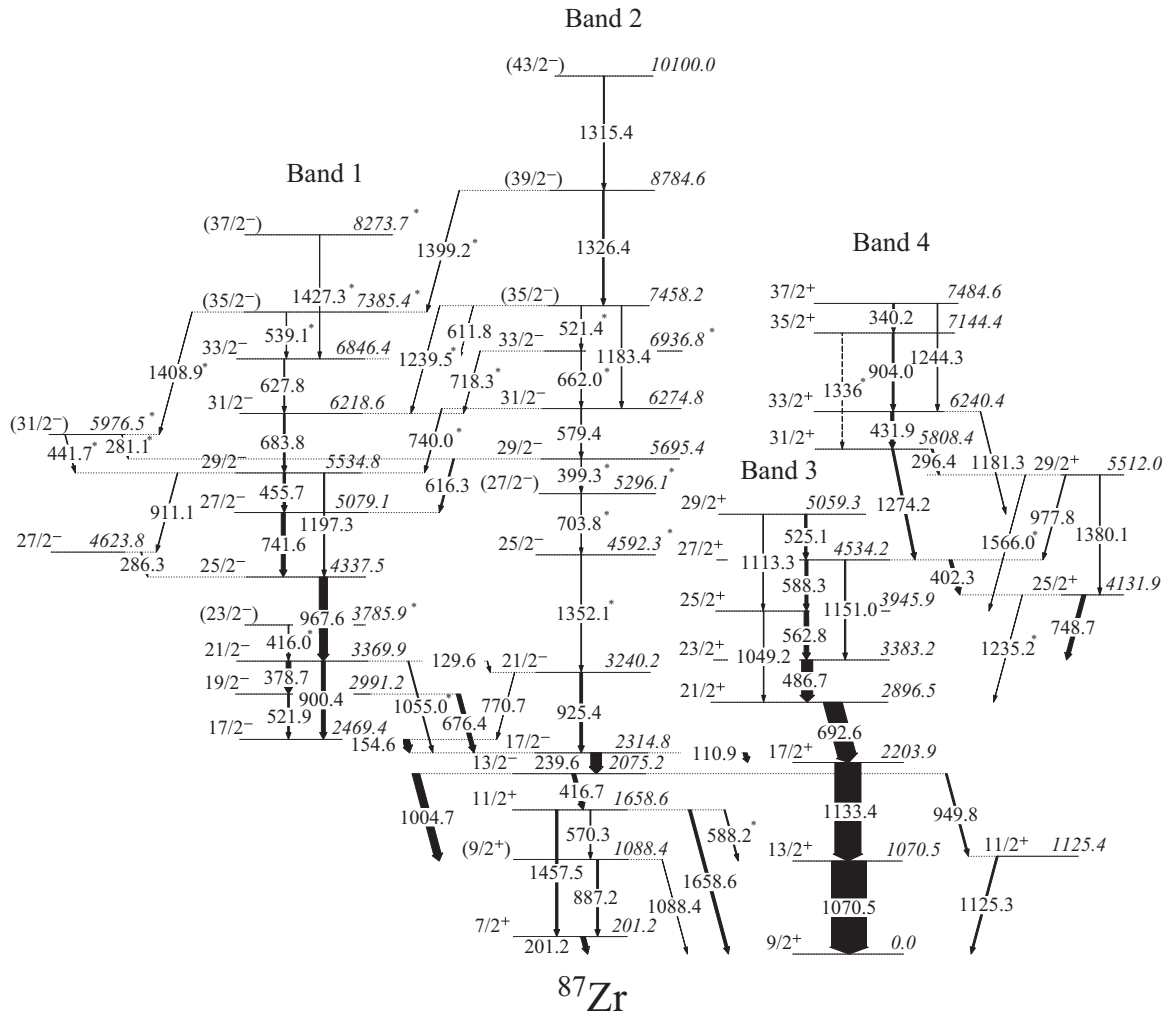

FIG. 1. Level scheme of ^{87}Zr deduced from the present work. The relative intensities of the transitions are indicated by the widths of the transitions. New transitions and levels are marked with asterisks.

first time in the present work. Also, a new 5976.5 keV state is observed to decay to states of bands 1 and 2 through the 441.7 and 281.1 keV γ rays, respectively (Fig. 1).

Support for the placement of the new transitions in bands 1 and 2 and the transitions linking the two bands is provided in the spectra shown in Figs. 2 and 3. Figure 2(a), which shows the low-energy part of the spectrum obtained from the sum of the double gates on (1133.4 + 110.9) and (1004.7 + 239.6) keV γ rays, confirms the placements of the 416.0 and 539.1 keV transitions in band 1. In addition, the spectrum in Fig. 2(a) also supports the placement of the new interband 281.1 and 441.7 keV γ rays deexciting the 5976.5 keV state. The latter level is connected by the new 1408.9 keV γ ray to the 7385.4 keV level. However, the γ ray is too weak to be observed in the double-gated spectrum shown in Fig. 2(b), the high-energy part of the same spectrum. It can, nevertheless, be observed in spectra gated by the 281.1 and 441.7 keV γ rays (not shown here). Figure 2(a) also confirms the placement of the hitherto uncertain 770.7 keV [29] and the new 718.3 keV transitions from the 3240.2 and 6936.8 keV states, respectively. The spectrum also confirms the assignment of the new 662.0 keV γ ray from the latter level belonging to band 2. The spectrum in Fig. 2(b) lends support to the assignment of the 1352.1 keV, $25/2_2^- \rightarrow 21/2_1^-$ transition in band 2 and the interband 1055.0, 1239.5, and 1399.2 keV γ rays from the 3369.9, 7458.2, and the 8784.6 keV states, respectively. Figures 2(c) and 2(d) show the low- and high-energy regions, respectively, of the spectra obtained from the sum of the two double-gated spectra with gates on the (967.6 + 627.8) and (683.8 + 627.8) keV γ rays. Figure 2(c) provides additional support for the assignment of the new 539.1 keV γ ray near the top of band 1 [also see Fig. 2(a)] and other previously reported transitions belonging to the two bands. The placement of the new 1427.3 keV transition at the top of band 1 is supported by Fig. 2(d). The figure also affirms the assignment of the interband 1399.2 keV transition connecting band 2 to band 1 [also see Fig. 2(b)].

Figure 3(a) shows the sum of the two spectra with gates on the 286.3 and 1197.3 keV transitions. Figures 3(b) and 3(c) show double-gated spectra with gates on the (239.6 + 1352.1) and (676.4 and 683.8) keV γ rays, respectively. The spectra in Figs. 3(a) and 3(c) provide support for the placement of

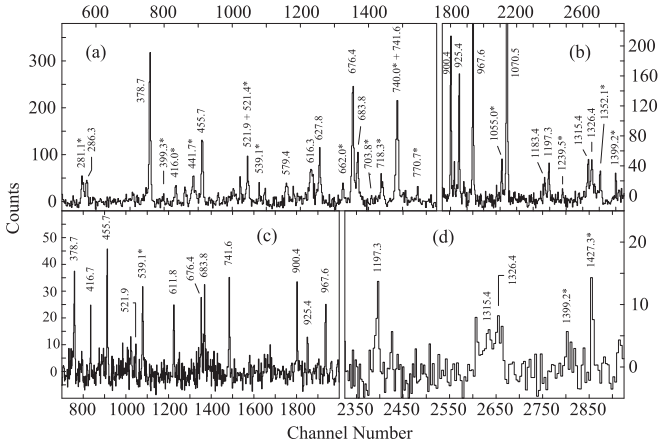

FIG. 2. Gated spectra in support of the placement of new transitions (marked with asterisk) in bands 1 and 2. (a) and (b) in the upper panel show the low- and high-energy regions, respectively, of the sum of the double-gated spectra gated by $(1133.4 + 110.9)$ and $(1004.7 + 239.6)$ keV γ rays. Panels (c) and (d) represent the low- and high-energy regions, respectively, of the sum of the double-gated spectra gated by $(967.6 + 627.8)$ and $(683.8 + 627.8)$ keV γ rays. All spectra are corrected for γ-ray relative efficiencies.

the interband 718.3 keV γ ray connecting the 6936.8 and 6218.6 keV states. In the former spectrum, a 721 keV γ ray (belonging to ^{88}Zr), marked u3 in Fig. 3(a), overlaps with the 718.3 keV γ ray. The spectrum in Fig. 3(a) also lends firm support in favor of the placement of another interband transition with energy 740.0 keV ($31/2^-_3 \rightarrow 29/2^-_1$), linking bands 2 and 1. The 740.0 keV γ ray, along with the previously reported 741.6 keV transition (see band 1), forms one of the four doublet pairs that have been assigned to ^{87}Zr. The other three pairs have energies 416.0 and 416.7, 521.4 and 521.9, and 588.2 and 588.3 keV. Incidentally, the lower-energy transition in each of these pairs has been observed for the first time in the present work. Evidence in favor of the placement of the 416.0 keV transition is presented in Fig. 2(a). Figures 3(a)

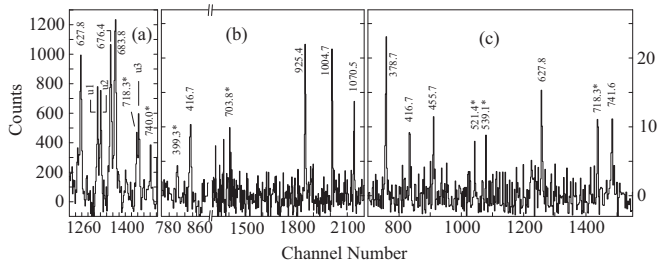

FIG. 3. Gated spectra in support of the placement of new transitions (marked with asterisk) in bands 1 and 2. The vertical axis for (a) is shown on the extreme left and those for (b) and (c) are indicated at extreme right. Panel (a) shows the sum of single gates on the 286.3 and 1197.3 keV transitions. Gamma rays marked u1 and u2 with energies 655 and 660 keV, respectively, belong to ^{85}Y and u3 with energy 721 keV belongs to ^{88}Zr. Panels (b) and (c) show double-gated spectra with gates on the $(239.6 + 1352.1)$ and $(676.4 + 683.8)$ keV γ rays, respectively. The spectra are corrected for γ-ray relative efficiencies.

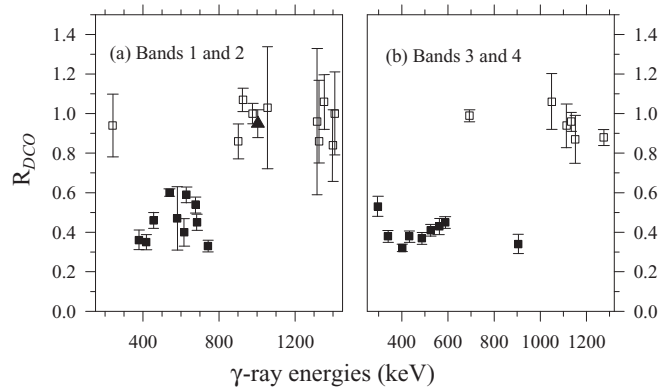

FIG. 4. Experimental DCO ratios for γ rays belonging to (a) bands 1 and 2 and (b) bands 3 and 4. Filled squares represent DCO ratios for $\Delta I = 1$ transitions and open squares represent DCO ratios for $\Delta I = 2$ transitions. The 1004.7 keV, $13/2^- \rightarrow 13/2^+$ γ ray (see Fig. 1) is a pure nonstretched dipole transition and its DCO ratio is represented by a filled triangle in (a). The DCO ratios were obtained by gating on stretched $E2$ transitions. The $R_{\rm DCO}$ results are given in the Supplemental Material [28].

and 3(c) give firm support in favor of the placements of the 740.0 and 521.4 keV γ rays, respectively. The 588.2 keV $11/2^+_2 \rightarrow 13/2^+$ γ ray is observed in the double-gated spectrum with gates on the 239.6 and 416.7 keV γ rays (gated spectrum not shown).

New transitions with energies 399.3 and 703.8 keV have been assigned to band 2 on the basis of the coincidence relationships presented in Fig. 3(b) [see also Fig. 2(a)]. The placement of the other new γ ray in band 2 with energy 1352.1 keV is based on the spectrum in Fig. 2(b). The 1352.1 keV γ ray is placed on top of the previously reported 3240.2 keV state deexcited by the 925.4 keV transition. The double-gated spectrum with gates on the 239.6 and 1352.1 keV γ rays [Fig. 3(b)] shows a strong 925.4 keV γ ray along with the weaker 399.3 and 703.8 keV γ rays. The order of placement of the γ rays is guided by their relative intensities.

Although Zhao *et al.* [20] have reported spins and parities (I^π) for a majority of the levels in ^{87}Zr, the I^π assignments adopted in the literature are mostly tentative. The I^π assignments adopted in a recent compilation of Nuclear Data Sheets [29] are tentative for all but the ground state and some low-energy states. In the present work, experimental $R_{\rm DCO}$ ratios have been determined for most of the γ rays belonging to bands 1–4, with the exception of the weakest ones, following the method described in Ref. [30] and outlined in Ref. [31]. These DCO ratios, determined mostly from gates on $E2$ transitions, are shown in Fig. 4 (also see Supplemental Material [28]) and are consistent with the spin assignments shown in Fig. 1. Firm spin values of $21/2^-$ and $25/2^-$, for example, have been assigned to the 3240.2 and the new 4592.3 keV state in band 2, respectively, on the basis of the present $R_{\rm DCO}$ results which suggest that the 925.4 and 1352.1 keV transitions depopulating the two states are stretched quadrupole in nature. The $I^\pi = 21/2^-$ for the 3240.2 keV level however contradicts the previously adopted spin of $(19/2^-)$ [29]. Only tentative I^π assignments are indicated in this work for states with

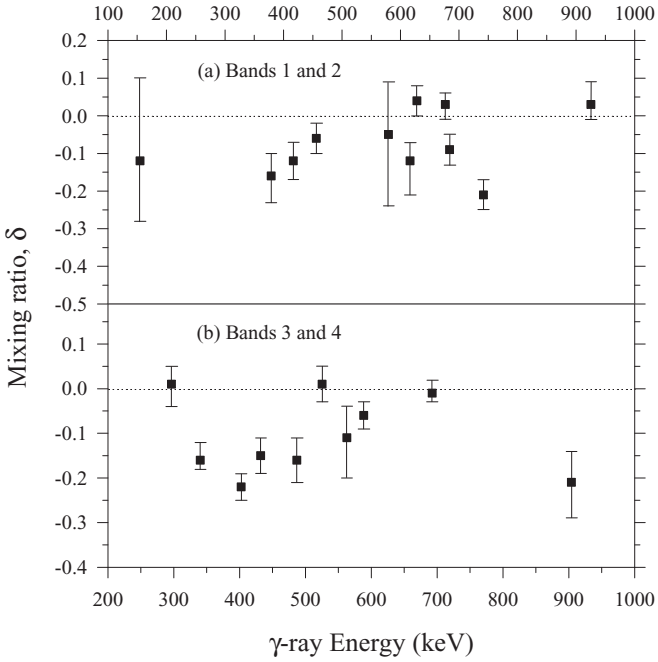

FIG. 5. Gamma-ray multipole mixing ratios δ for (a) bands 1 and 2 and (b) bands 3 and 4. Only the 925.4 keV γ ray in (a) and the 692.6 keV γ ray in (b) are electric quadrupole in nature. Mixing ratio results are given in the Supplemental Material [28].

$E_x \geqslant 7$ MeV in bands 1 and 2 and the 5296.1 keV state in band 2 due to the weak observed intensity of the transitions of interest. Gamma-ray multipole mixing ratios δ for transitions in bands 1 and 2, obtained from the experimental DCO ratios, are plotted as a function of γ-ray energies in Fig. 5(a). It is noteworthy that most of the $\Delta I = 1$ transitions belonging to bands 1 and 2 (e.g., the 378.7, 416.7, 455.7, 579.4, 616.3, 683.8, and 741.6 keV γ rays) have $\delta_{E2/M1}$ values that are negative. Only the 627.8 and 676.4 keV γ rays have small positive values of $\delta_{E2/M1}$.

B. Bands 3 and 4

Several states, connected by strong $\Delta I = 1$ transitions and weak crossover $E2$ γ rays, have been grouped into two short sequences based on their properties and are labeled bands 3 and 4 in Fig. 1. This is discussed subsequently in this text under Sec. IV (Discussion). Placements of the transitions in these two sequences are supported by the gated spectra shown in Fig. 6 which is the sum of the two spectra with double gates on $(1070.5 + 431.9)$ and $(1133.4 + 431.9)$ keV γ rays. Figure 6(a) shows the low-energy part of this spectrum ($250 \leqslant E_\gamma \leqslant 1200$ keV) while Fig. 6(b) shows the spectrum for $1200 \leqslant E_\gamma \leqslant 1600$ keV. All γ rays belonging to bands 3 and 4 (see Fig. 1) have been previously reported although there are a few changes in the present level scheme in comparison to that reported earlier [20]. As already mentioned, a single sequence of positive-parity states, reported earlier [20], has been grouped into bands 3 and 4. In the latter band, the 1244.3 keV transition from the 7484.6 keV level, reported to be tentative in Ref. [20], has been confirmed in the present

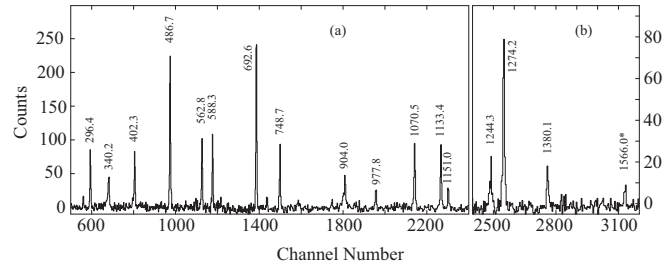

FIG. 6. Gated spectra in support of the placement of new transitions (marked with asterisk) in bands 3 and 4. Figure shows the sum of the double-gated γ-ray spectra with gates on $(1070.5 + 431.9)$ and $(1133.4 + 431.9)$ keV. Panel (a) shows the low-energy part of the summed spectrum for γ rays with energies up to 1200 keV and panel (b) shows the spectrum for the higher-energy γ rays. The spectra are corrected for γ-ray relative efficiencies.

work. The transition is clearly observed in the spectrum shown in Fig. 6(b). Also, the 1244.3 keV γ ray is observed in spectra with gates on the 296.4, 1274.2 keV and other lower-lying (relative to 1244.3 keV γ ray) transitions but is not seen in the spectra gated by the 340.2 or 904.0 keV γ rays. These gated spectra are not shown here. A more significant change relates to the ordering of the 340.2 and 904.0 keV transitions. Relative intensity considerations suggest that the 340.2 keV γ ray should be placed above the 904.0 keV transition as shown in Fig. 1. The relative intensities of the 340.2 and 904.0 keV transitions, determined from the double-gated spectrum with gates on $(1070.5 + 1133.4)$ keV γ rays, are 5.8 ± 0.4 and 7.1 ± 0.5 units, respectively (see Table IV in the Supplemental Material [28]). This alteration in the level scheme leads to the new level at 7144.4 keV in band 4. A new 1336 keV transition is tentatively proposed to connect the new level at 7144.4 keV and the 5808.4 keV state. The weak 1336 keV γ ray is observed in spectra gated by the 1274.2 and 340.2 keV transitions but not in any of the double gates. The spectrum in Fig. 6 does not show the weak 1049.2 and 1235.2 keV γ rays.

In addition to bands 3 and 4, two other positive-parity states with energies 4131.9 and 5512.0 keV have been observed. These are strongly linked to bands 3 and 4.

A tentative $I^\pi = (21/2)^+$ is adopted in the literature for the 2896.5 keV bandhead for band 3 [29]. The stretched quadrupole nature of the 692.6 keV transition depopulating the state ($R_{\rm DCO} = 0.99 \pm 0.03$ in $E2$ gate, $\delta_{M3/E2} = -0.01^{+0.03}_{-0.02}$) confirms the I^π assignment. Firm spin assignments are proposed for states up to 5808.4 keV ($I^\pi = 31/2^+$) on the basis of the quadrupole nature of the crossover 1049.2, 1151.0, 1113.3, and 1274.2 keV transitions inferred from the measured $R_{\rm DCO}$ values. Firm spin values of $33/2^+$, $35/2^+$, and $37/2^+$ are also proposed for the 6240.4, 7144.4, and 7484.6 keV states based on the inferred $M1 + E2$ character of the 431.9, 904.0, and 340.2 keV γ rays depopulating the three states [28]. The DCO ratios for the nine $\Delta I = 1$ transitions with energies 296.4, 340.2, 402.3, 431.9, 486.7, 525.1, 562.8, 588.3, and 904.0 keV, belonging to bands 3 and 4, derived from gates on $E2$ transitions, lie within the range 0.30–0.55 [Fig. 4(b)]. The corresponding multipole mixing ratios $\delta_{E2/M1}$

TABLE I. Present experimental results on level energies (E_x), γ-ray energies (E_γ), spins of the initial (I_i^π) and final states (I_f^π), γ-ray branching ratios (B.R.), multipole mixing ratios $\delta_{E2/M1}$, feeding from continuum as part of total feeding in (%), level lifetimes (τ), and reduced transition probabilities $B(M1)$ and $B(E2)$ in ^{87}Zr. The tentative 1336 keV γ ray is not included in the table. [1 Weisskopf unit (W.u.) = $22.9 \times 10^{-4} e^2 b^2$]

Band	E_x (keV)	E_γ (keV)	$I_i^\pi \rightarrow I_f^\pi$	B.R. (%)	Mixing ratio $\delta_{E2/M1}$	Feeding from continuum (%)	Level lifetime τ (ps)	$B(M1)$ (μ_N^2)	$B(E2)$ (W.u.)
3	3383.2	486.7	$11.5^+ \rightarrow 10.5^+$	100 ± 3.8	-0.16 ± 0.05	18.1	$0.62^{+0.19}_{-0.13}$	0.77 ± 0.19	
	3945.9	562.8	$12.5^+_1 \rightarrow 11.5^+$	88.6 ± 6.5	$-0.11^{+0.07}_{-0.09}$	73.5	$0.35^{+0.11}_{-0.08}$	$0.80^{+0.24}_{-0.19}$	
		1049.2	$12.5^+_1 \rightarrow 10.5^+$	11.4 ± 1.0	$E2$				$9.2^{+2.7}_{-2.2}$
	4534.2	402.3	$13.5^+ \rightarrow 12.5^+_2$	32.1 ± 2.0	-0.22 ± 0.03	25.3	$0.25^{+0.09}_{-0.07}$	$1.07^{+0.42}_{-0.28}$	
		588.3	$13.5^+ \rightarrow 12.5^+_1$	48.0 ± 2.0	-0.06 ± 0.03			$0.53^{+0.21}_{-0.14}$	
		1151.0	$13.5^+ \rightarrow 11.5^+$	19.9 ± 1.2	$E2$				$14.1^{+5.5}_{-3.7}$
	5059.3	525.1	$14.5^+_1 \rightarrow 13.5^+$	89.3 ± 4.8	0.01 ± 0.04	76.7	$1.19^{+0.15}_{-0.13}$	$0.29^{+0.04}_{-0.03}$	
		1113.3	$14.5^+_1 \rightarrow 12.5^+_1$	10.7 ± 1.9	$E2$				1.9 ± 0.2
4	5808.4	296.4	$15.5^+ \rightarrow 14.5^+_2$	45.4 ± 2.6	$0.01^{+0.04}_{-0.05}$	100	1.91 ± 0.14	$0.52^{+0.04}_{-0.03}$	
		1274.2	$15.5^+ \rightarrow 13.5^+$	54.6 ± 3.5	$E2$				3.0 ± 0.2
	6240.4	431.9	$16.5^+ \rightarrow 15.5^+$	83.4 ± 3.4	-0.15 ± 0.04	66.2	$0.33^{+0.07}_{-0.05}$	1.74 ± 0.3	
		1181.3	$16.5^+ \rightarrow 14.5^+_1$	16.6 ± 1.4	$E2$				7.8 ± 1.4
	7144.4	904.0	$17.5^+ \rightarrow 16.5^+$	100 ± 7.0	$-0.21^{+0.07}_{-0.08}$	100	0.55 ± 0.19	$0.13^{+0.07}_{-0.03}$	
	7484.6	340.2	$18.5^+ \rightarrow 17.5^+$	69.9 ± 4.8	$-0.16^{+0.04}_{-0.02}$	100	<1.1	>0.90	
		1244.3	$18.5^+ \rightarrow 16.5^+$	30.1 ± 2.4	$E2$				>3.3

are negative for all but the 296.4 and 525.1 keV γ rays [Fig. 5(b)] corresponding to $E2$ admixtures that are less than 5%. This situation is similar to that observed for bands 1 and 2 discussed earlier (see Sec. III A).

Arnell *et al.* [21] reported half-lives of the order of a few nanoseconds for low-energy states with $E_x \leqslant 2.5$ MeV in ^{87}Zr from electronic timing studies. They also reported subpicosecond lifetimes for states up to about 5 MeV from centroid shifts of the Doppler-shifted γ-ray lines. Lifetimes have also been reported for several low-energy states using the recoil distance method [22].

In the present work, level lifetimes have been measured for all states with $E_x \geqslant 3383.2$ keV belonging to the positive-parity bands 3 and 4 from DSA data using the analysis package LINESHAPE [27]. The results are summarized in Table I. Figure 7 shows the gated DSA spectra for the 486.7, 562.8, 588.3, and 525.1 keV γ rays belonging to band 3, observed at 90° and 157° to the beam direction. The continuous lines in the figure are theoretical fits to the experimental data using the code LINESHAPE [27].

In the line shape analysis, the details of the slowing-down history of the recoils, moving with an initial recoil velocity of $\beta = 0.03$ in the gold backing, have been simulated using a Monte Carlo technique which involved 10 000 histories with a time step of 0.002 ps. The level lifetimes are corrected for the effects of delayed feedings from the discrete states as well as the unobserved direct feedings from the continuum. The term "side feeding" is used to refer to the sum of these two feedings to each of the states. The direct-feeding time from the continuum was constrained to be zero for an excitation energy of $E^* = 9.2$ MeV, deduced from the relation $E^* = E^{CM}_{\rm proj} + Q - N_n E_n - N_p E_p$, and increased by 0.05 ps per MeV of deexcitation. Here $Q = -39.5$ MeV is the Q value of the reaction ^{60}Ni(^{31}P, $3pn$), N_n and N_p are the numbers of emitted neutrons and protons, and E_n, E_p are the average center-of-mass energies of the neutrons and protons obtained from statistical model calculations, respectively.

The line shape analysis was started with the highest observed state at 7484.6 keV belonging to band 4 using the code LINESHAPE. In the absence of information regarding discrete feeding(s) from the top, only an upper limit of lifetime $\tau <$ 1.1 ps is inferred for this state. The inherent assumption in stating an upper limit is that the discrete feeding times are nonzero and possibly slower than the direct-feeding (from the continuum) time of 0.085 ps for the 7484.6 keV state, derived as described above. The upper limit of the lifetime for the 7484.6 keV level is then used as an input parameter in the fitting procedure for estimation of the lifetime of the next lower state at 7144.4 keV.

The procedure is continued for the remaining states whereby the lifetimes of the 5808.4 and 6240.4 keV states in band 4 and the 3383.2, 3945.9, 4534.2, and 5059.3 keV states belonging to band 3 have been determined (see Table I). As mentioned above, the lifetimes are corrected for the effects of feedings from both higher-energy discrete states as well as direct-feedings from the continuum. In each case, feedings other than the one from the next higher state within the band, if any, are included in the side feeder for which the effective feeding time is taken as the weighted average of the individual feeding times weighted by their respective relative intensities. The strong feeding to the 3383.2 keV level through the 748.7 keV transition (see Fig. 1), for example, has been accounted for in this way using the previously reported lifetime of 1.15 ± 0.29 ps for the 4131.9 keV state

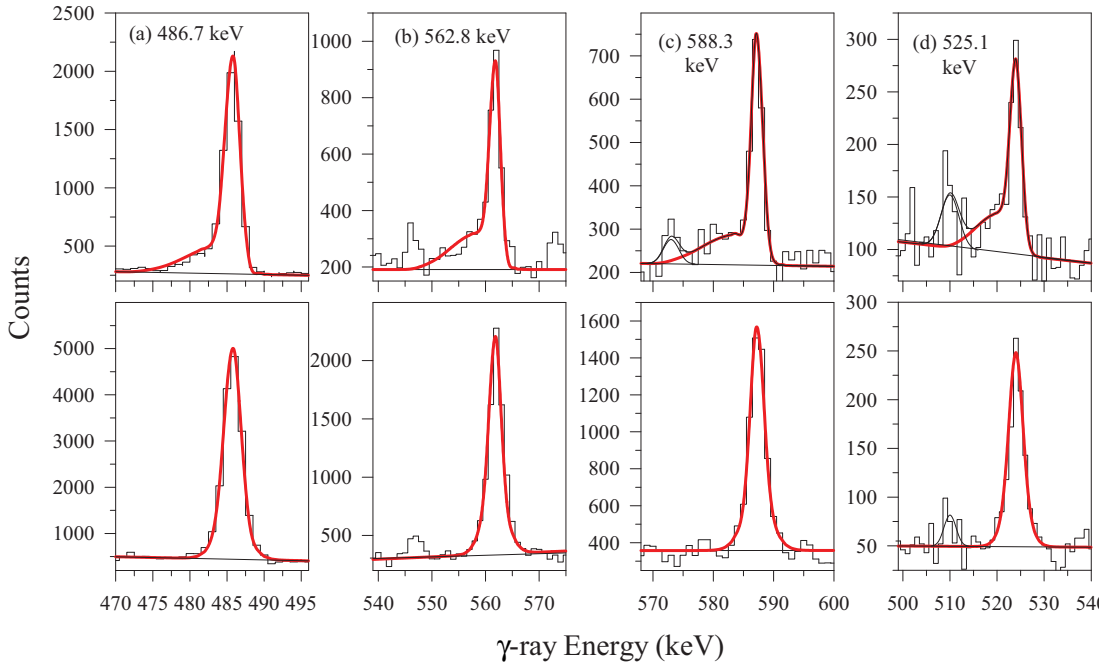

FIG. 7. DSA line shapes for the 486.7, 562.8, 588.3, and 525.1 keV γ rays belonging to band 3 at 90° (bottom panels) and 157° (top panels) to the beam direction. The spectra in (a), (b), and (c) are from gates on lower-lying $E2$ γ rays and the spectra in (d) are gated by the 486.7 keV dipole γ ray. The bold lines are the calculated fits to the experimental data using the code LINESHAPE [27]. Weak contaminant peaks present in the spectra in (c) and (d) are also included in the fits.

[21]. The relatively weaker feedings from the 5512.0 keV state to the 3945.9 and 4534.2 keV states (Fig. 1) are also considered in a similar way. In the latter case, the 5512.0 keV state (with no previous lifetime information) was assumed to have a mean life of 1.00 ± 0.25 ps, comparable to that for the 4131.9 keV state reported earlier. Relative intensity errors, errors in the lifetimes of the feeding states, and an assumed 30% uncertainty in the feeding time from the continuum have been included in the errors assigned to the level lifetimes.

It may be mentioned in this context that although the feedings from the discrete states are relatively slower compared to the direct feedings from the continuum (continuum feeding times lie within 0.09–0.29 ps), the intensities of the latter constitute the dominant feeding component (varying from 66% to 100%) for all but the 3383.2 and 4534.2 keV states (see Table I). For the two latter states, the feeding from the continuum accounts for about 18% and 25% of the total side feeding, respectively.

Arnell *et al.* [21] have previously reported lifetimes for three of the eight states for which measurements are reported in the present work. Of these, only the value reported for the 3945.9 keV state in Ref. [21] is in agreement, within errors, with the present result. The lack of consistency between the two data sets can probably be related to the uncertainties involved in the earlier results. As noted by Arnell *et al.* [21], the presence of neighboring contaminant γ-ray lines made the determination of centroid shifts difficult and somewhat uncertain. Besides, the authors noted that the level lifetimes are all based on the assumption that the unobserved feeding is extremely fast and thus they at least represent upper limits.

IV. DISCUSSION

The nuclei in the $A = 80$–90 mass region are in general more influenced by variations in the neutron number N than the proton number Z. Isotones of different Z across this mass region have nearly similar structural features while nuclear species with different N have significantly dissimilar properties. Thus, the low-energy states in ^{87}Zr up to an excitation energy of about 3 MeV are broadly similar to those in the two neighboring $N = 47$ isotones ^{85}Sr (see Fig. 2 in [16]) and ^{89}Mo (see Fig. 4 in [32]) and are all spherical in nature. Small experimental $B(E2)$ values adopted in the literature [29] for the $E2$ transitions deexciting the $13/2^+$, $17/2^+$, and $21/2^+$ states in ^{87}Zr are clearly suggestive of the spherical nature of the low-energy states.

A. Bands 1 and 2

A comparison of the sequence built on the $13/2^-$, 2075.2 keV state in ^{87}Zr, labeled band 2 in Fig. 1, with similar bands in the two $N = 47$ isotones ^{85}Sr and ^{89}Mo is shown in Fig. 8. The near-linear relationship between the excitation energies in ^{87}Zr and those in ^{85}Sr and ^{89}Mo establishes the close structural resemblance of band 2 in ^{87}Zr with the ones in the two neighboring $N = 47$ isotones. This, in effect, also lends strong support to the new experimental results obtained for band 2 in the present work related to the placement of

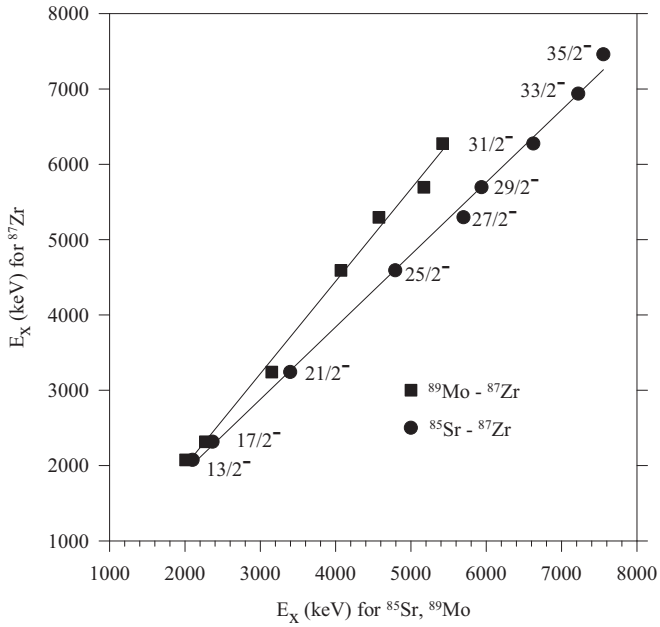

FIG. 8. Plot of the excitation energies (E_x) of the states belonging to band 2 in ^{87}Zr, established in the present work, versus the excitation energies of similar negative-parity bands in ^{85}Sr [16] and ^{89}Mo [32].

new transitions that lead to new levels at 4592.3, 5296.1, and 6936.8 keV and their spin-parity assignments. The $B(E2)$ values for the 239.6 and 925.4 keV transitions from the 2314.8 and 3240.2 keV states, estimated to be 8.2 ± 0.4 and 10.7 ± 2.2 W.u., respectively, using the lifetime results reported in the literature [29], suggest a weak collectivity for the low-energy states of band 2. Similarly small values of transition probabilities have been previously reported for an analogous band in ^{83}Kr [18]. Probable configuration for band 2 in ^{87}Zr could involve the proton configuration $\pi[(p_{3/2}f_{5/2}p_{1/2})^{-1} \otimes g_{9/2}]$ coupled to $(\nu g_{9/2})^{-3}$ or $\nu[(g_{9/2})^{-2} \otimes p_{1/2}]$ coupled to zero proton excitation.

The other negative-parity sequence in ^{87}Zr, namely band 1 built on the $17/2^-_2$ state at 2469.4 keV, has no analog in either of the two neighboring $N = 47$ isotones ^{85}Sr and ^{89}Mo. A somewhat similar sequence of three transitions, also built on a $17/2^-$ state, is however reported in ^{83}Kr [18]. Band 1 in ^{87}Zr is unique in the sense that the sequence is rather long consisting of a large number of both $\Delta I = 1$ and 2 transitions, extending up to a fairly high excitation energy of 8273.7 keV [$I^\pi = (37/2^-)$]. Level lifetimes are expected to be long as the deexciting transitions do not show a measurable Doppler shift indicating that collectivity is small as for band 2. The large number of interband transitions connecting bands 1 and 2 also suggests that the two structures may have significant overlap in their configurations.

B. Bands 3 and 4

The majority of the positive-parity states in ^{87}Zr have been grouped into two short sequences labeled bands 3 and 4 in Fig. 1 on the basis of their decay patterns. As seen from the figure, all states in the two bands up to the highest observed level at 7484.6 keV are connected by strong dipole transitions (the crossover $E2$ γ rays are weaker in intensity by a factor of up to eight) with the exception of the $31/2^+$ state and the yrast $29/2^+$ state. The two latter states are not connected. Rather than decaying to the yrast $29/2^+$ state, the $31/2^+$ state decays to a second $29/2^+$ state at 5512.0 keV. In fact, the $31/2^+$ state decays predominantly by the strong 1274.2 keV $E2$ transition to the $27/2^+$ state in band 3. The 296.4 keV dipole γ ray from the same level is relatively weaker (see Table I). More significantly, the reduced transition probabilities $B(M1)$ and $B(E2)$, which follow a decreasing trend with increasing spin for states assigned to band 3 (discussed hereinafter), show an abrupt increase for the $31/2^+$ level. Evidently, the configuration of the latter state is different from that of the lower-lying states. Quite justifiably therefore, the five states with spins from $21/2^+$ to $29/2^+$ are assigned to one band (band 3) while the four higher-energy states with spins up to $37/2^+$ to another (band 4).

Short sequences built on $21/2^+$ states and extending up to $29/2^+$ and $(31/2^+)$ have also been observed in the two neighboring $N = 47$ isotones, namely ^{83}Kr [18] and ^{85}Sr [16], respectively. The level energies in both sequences, like the states belonging to band 3 in ^{87}Zr, approximately follow the $I(I + 1)$ rule. However, in contrast to ^{87}Zr, crossover $E2$ transitions are observed in neither of the two previously reported bands.

The low intensity of the crossover $E2$ transitions and the small $B(E2)$ values (Table I) suggest that states of band 3 are weakly deformed. An inspection of the proton single-particle energies for $Z = 40$ (as in Figure 4 in Ref. [33]) at quadrupole deformations of $\epsilon_2 \simeq -0.10$ shows that the Fermi surface lies in a region where the $1f_{5/2}$, $2p_{1/2}$, and $1g_{9/2}$ orbitals lie close to each other. This suggests that the positive-parity band 3 in ^{87}Zr could have a probable configuration of $\pi[(p_{3/2}f_{5/2}p_{1/2})^{-2}(g_{9/2})^2] \otimes \nu[(g_{9/2})^{-1}]$. The occupation of the $\pi g_{9/2}$ orbital in ^{87}Zr (as also in ^{83}Kr and ^{85}Sr) is due to the proximity of this orbital to the (fp) orbitals in the single-particle energy level diagram. Furthermore, although there are three neutron holes in the $N = 50$ shell for ^{87}Zr, two of these may align antiparallel to each other and therefore would have no contribution to the possible existence of a shears mechanism [34] in generating angular momentum in the band. It is worth noting in this context that analogous positive-parity bands in the $N = 47$ isotones ^{83}Kr and ^{85}Sr have been previously proposed to have a similar $\pi(g_{9/2})^2 \otimes \nu(g_{9/2})^{-1}$ configuration with a single neutron hole in the $g_{9/2}$ orbital [16,18]. A configuration involving three neutron holes in the $N = 50$ shell can generate angular momentum that is considerably higher than the maximum spin observed for the positive-parity bands in all these $N = 47$ isotones.

Tilted axis cranking calculations for ^{85}Sr, based on this configuration, show an energy minimum at $(\epsilon_2, \gamma) = (0.11, 60^\circ)$ [16] in support of an oblate shape. It is possible that the negative sign of the mixing ratio $\delta_{E2/M1}$ for most of the γ rays belonging to band 3 in ^{87}Zr also represents an oblate shape for the band. With a sizable proton contribution to the wave function and considering the large positive single-particle g factor $= +1.27$ for the $\pi g_{9/2}$ orbital [35],

$g_K - g_R$ (where $g_R \approx Z/A$) is expected to be positive for the states of band 3. Hence, $\mathrm{sgn}(\delta_{E2/M1}) = \mathrm{sgn}(Q_o)$; i.e., the sign of the mixing ratio is directly related to the sign of the quadrupole moment Q_o or the nuclear shape. A sizable proton contribution to the wave function, as for band 3 in ^{87}Zr, has been sought to account for large positive particle g factors in ^{86}Zr [36]. The oblate shape requires that the two proton particles in the $g_{9/2}$ orbital are deformation-aligned occupying high-Ω states while the proton quasiparticles in the fp orbitals and the neutron-hole(s) in the $g_{9/2}$ orbital are rotation-aligned occupying low-Ω states. This leads to a near-perpendicular coupling of the angular momentum vectors of the proton and neutron quasiparticles near the bandhead. Band 3 is therefore expected to possess properties similar to those for shears structures.

Calculations have been performed within the framework of the semiclassical model of shears mechanism formulated by Macchiavelli *et al.* [37]. The shears angle θ for a given state with spin I in this model is the angle between the two spin vectors $j_\parallel$ and $j_\perp$, parallel and perpendicular to the symmetry axis, respectively, and is given by

$$\cos\theta = \frac{I_{sh}(I_{sh}+1) - j_\parallel(j_\parallel+1) - j_\perp(j_\perp+1)}{2[j_\parallel(j_\parallel+1)j_\perp(j_\perp+1)]^{1/2}}. \quad (1)$$

Here, $\vec{j}_\parallel + \vec{j}_\perp = \vec{I}$ and I_{sh} is the shears contribution to I. The theoretical $B(M1)$ and $B(E2)$ values within the framework of this model are given by

$$B(M1, I \to I-1) = \frac{3}{8\pi} g_{\mathrm{eff}}^2 j_\pi^2 \sin^2\theta_\pi [\mu_N^2], \quad (2)$$

$$B(E2, I \to I-2) = \frac{5}{16\pi}(eQ)_{\mathrm{eff}}^2 \frac{3}{8}\sin^4\theta_\pi [e^2b^2]. \quad (3)$$

Here, the proton angle θ_π, given by $\tan\theta_\pi = j_\perp \sin\theta/(j_\parallel + j_\perp\cos\theta)$, is the angle between the proton spin vector j_π $(=j_\parallel)$ and the total spin I. The effective gyromagnetic factor g_{eff} is the difference of the g factors for the quasiparticles that form the the two blades of the shear.

A proton spin vector $j_\pi = 4\,\hbar$ is assumed for the two protons in the large-Ω $\pi g_{9/2}$ orbital. Although the coupling of two $g_{9/2}$ protons can result in a maximum spin of 8 $\hbar$, their occupation of the large-Ω states in the $\pi g_{9/2}$ subshell can lead to a small spin value. Thus, assuming a spin vector $j_\pi = j_\parallel = 4\,\hbar$ and a near-perpendicular coupling of the spin vectors at the bandhead, a spin $j_\perp = 8.5\,\hbar$ (with contributions from the $g_{9/2}$ neutron and proton quasiparticles in the fp orbitals) is deduced from Eq. (1) so as to reproduce the bandhead spin of $21/2\,\hbar$. These $j_\parallel$ and $j_\perp$ are then used to calculate the shears angle θ and hence θ_π for each of the higher spin states in band 3 (see [37]).

Figure 9 shows the arrangement of the spin vectors $j_\parallel$ and $j_\perp$ for band 3 at low spin (continuous lines) at the bandhead with $I = 21/2\,\hbar$ and at high spin $I = 29/2\,\hbar$ (dashed lines) at the top of the band. The shears angle θ (=75.6° at $I = 21/2\,\hbar$ and 32.2° at $I = 29/2\,\hbar$) and the proton angle θ_π (=53.4° at $I = 21/2\,\hbar$ and 22.1° at $I = 29/2\,\hbar$) are indicated. The components of the magnetic dipole moments perpendicular to I at $I = 23/2$ (continuous line) and $I = 29/2$ (dashed line) are also shown in the figure.

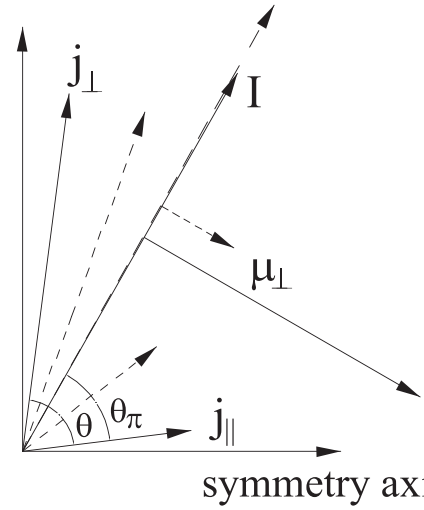

FIG. 9. Figure shows the angular momentum vectors $j_\parallel = 4\,\hbar$ and $j_\perp = 8.5\,\hbar$ for band 3 at the bandhead (continuous lines) at spin $I = 21/2$ and for the state at $I = 29/2$ (dashed lines). The corresponding vector sums I are also shown. The configuration for band 3 is given in the text. The shears angle θ (=75.6°) and the proton angle θ_π (=53.4°) at the bandhead are indicated. Also shown are the components of the magnetic dipole moments perpendicular to I at $I = 23/2$ (continuous line) and $I = 29/2$ (dashed line).

The maximum spin that can be generated from the fully closed blades of the shears, i.e., $j_\parallel + j_\perp$, is 12.5 $\hbar$ while the band is observed up to 14.5 $\hbar$. The remaining 2 units of angular momentum apparently arise from collective rotation of the core (I_{core}) giving rise to the weak crossover quadrupole γ rays.

A comparison of the calculations based on the semiclassical model of Macchiavelli *et al.* [37] with the present experimental results, presented in Fig. 10, provides useful insights into the structure of band 3. The theoretical $B(M1)$ and $B(E2)$ values have been calculated using Eqs. (2) and (3).

Figures 10(a) and 10(b) show the plots of the experimental reduced transition probabilities $B(M1)$ and $B(E2)$ as a function of the level spin. The continuous lines in these plots represent the fits of the theoretical transition probabilities, derived from Eqs. (2) and (3), to the experimental results. The fit shown in Fig. 10(a) yields an effective g factor = 0.94. The decreasing trend of the measured $B(M1)$ values with increasing spin signify the role of the shears mechanism in generating angular momentum. The proton angle θ_π decreases as a consequence of the step-by-step closing of the two blades of the shears (in order to generate higher angular momentum states) resulting in declining $B(M1)$ values. The $B(E2)$ values [see Fig. 10(b)] are small, the largest value being $B(E2;\ 27/2^+ \to 23/2^+) = 14.1^{+5.5}_{-3.7}$ W.u., and are a clear manifestation of weak collectivity associated with shears bands. Ideally, the $B(E2)$ values for a shears band go to zero at the top of the band where the charge distribution becomes symmetric around the rotation axis. In addition, crossover $E2$ transitions are very weak or absent leading to large $[B(M1)/B(E2)]$ ratios (usually >20 μ_N^2/e^2b^2). In the case of band 3, $[B(M1)/B(E2)]$ ratios are indeed large [see

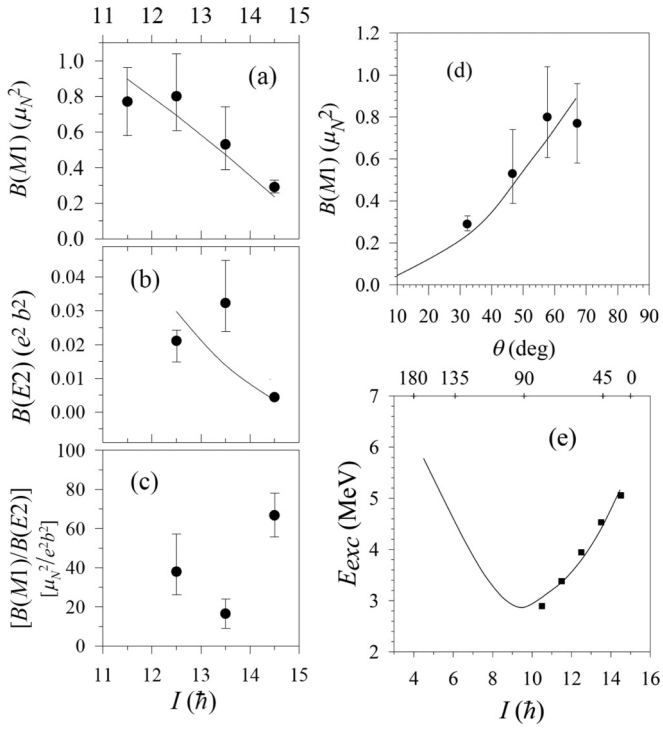

FIG. 10. Plots of experimental (a) $B(M1)$, (b) $B(E2)$ values and (c) $[B(M1)/B(E2)]$ ratios as functions of level spin for states of band 3. The continuous lines in (a) and (b) are fits of the reduced transition probabilities calculated from the semiclassical model of Macchiavelli *et al.* [37] to the experimental results. Plot (d) shows the $B(M1)$ values as a function of the shears angle θ. The continuous line represents the theoretical $B(M1)$ values fitted to the observed results. The plot in (e) presents the experimental excitation energy of band 3 versus level spin. The corresponding shears angles are shown along the axis at the top. The full line is the interaction energy according to Eq. (4) in the text.

Fig. 10(c)] and the $B(E2)$ for the $29/2^+ \rightarrow 25/2^+$ transition at the top of the band is close to zero (1.9 ± 0.2 W.u.) (see Table I). However, the $B(E2)$ values for the lower-lying transitions are not insignificant. The presence of crossover $E2$ γ rays, albeit with a low intensity, and the small but significant $B(E2)$ values measured for $E2$ transitions from two of the states in band 3 are attributable to a collective rotation of the core.

Figure 10(d) shows a plot of the experimental $B(M1)$ values as a function of the shears angle θ for band 3. The continuous line shows the calculated $B(M1)$ values for $g_{\rm eff} = 0.94$, derived from the fit shown in Fig. 10(a). The good agreement of the experimental and the calculated $B(M1)$ plots in Figs. 10(a) and 10(d) shows that the states of band 3 are described reasonably well by the shears mechanism based on the schematic model of the coupling of the two spin vectors with $j_\parallel = 4\ \hbar$ and $j_\perp = 8.5\ \hbar$.

The effective interaction between the two blades of the shears may be expanded as

$$V_{12}(\theta) = V_o + V_2[P_2(\cos\theta)] + \cdots . \quad (4)$$

The interaction energy is minimum at $\theta = 90^\circ$ for positive values of the parameter V_2 which corresponds to a particle-hole type of interaction. Figure 10(e) shows a plot of the experimental level energies for band 3 as a function of spin (the corresponding angles θ are indicated at the top of this figure) to which is fitted the P_2-type interaction given by Eq. (4) for $j_\parallel = 4\ \hbar$ and $j_\perp = 8.5\ \hbar$ with V_o and V_2 as free parameters. The solid curve represents the fit for $V_o = 3.95$ MeV and $V_2 = 2.17$ MeV. The positive value of V_2 indicates that the interaction is of the particle-hole type. The minimum at $\theta = 90^\circ$ corresponds to a spin close to but less than the bandhead spin of $21/2\ \hbar$. The agreement between the experimental data and the P_2-type interaction is good and the general trend is well reproduced. The unfavored side of the parabola represents states for which the two shears arms couple to angles greater than 90°. Although such states are possible in principle, they are difficult to observe in heavy-ion induced reactions since their spins decrease with increasing excitation energy.

Considering that $V_2 = 2.17$ MeV and there are two protons in the parallel arm (parallel to the symmetry axis) and at least 3 quasiparticles in the perpendicular arm, the interaction strength per quasiparticle pair is about 362 keV. The strength of the effective interaction has been previously investigated in the Pb region [38] and for nuclei in the $A = 110$ mass region [39–41]. However, such studies are not reported in the $A = 80$–90 mass region precluding a comparison of the interaction strength determined in the present work with earlier results. Although the interaction strength is expected to scale as A^{-1}, unexpectedly similar values of V_2 and strengths per proton-neutron pair have been reported in nuclei belonging to widely different mass regions. Shears bands in ^{197,198}Pb are reported to have an average $V_2 = 2.3$ MeV corresponding to a strength of 400–600 keV per proton-neutron pair [38] while those in ^{108,110}Cd and ^{111}In also have interaction strengths of the order of 500 keV per particle pair [39–41]. A comment on the interaction strength derived for ^{87}Zr in the present work is therefore unwarranted.

States of band 4 are possibly generated from the aligned configuration of band 3, namely $\pi(g_{9/2})^2 \otimes \nu(g_{9/2})^{-3}$. The fully aligned configuration will give rise to a spin of $37/2^+$, the same as that of the topmost state at 7484.6 keV in this band. The strong decay out of band 4 into states of band 3 arise from the overlap of their respective configurations. Significant structural information for the states of band 4 could not be deduced from the present data. A study of the level lifetimes indicates that the states are weakly deformed [small $B(E2)$ values] and the $M1$ transitions are strongly enhanced as in the case of band 3. The level spacings are however irregular and do not lend support to the interpretation of the states as arising from magnetic rotation.

V. CONCLUSION

Excited states of ^{87}Zr, produced in the reaction ^{60}Ni(^{31}P, $3pn$) at a beam energy of 112.5 MeV, have been studied in the present work. The decay schemes for the two negative-parity sequences band 1 and band 2 have been upgraded with the help of three- and higher-fold γ-ray coincidence data.

While band 1 has been extended up to 8273.7 keV and spin $(37/2^-)$ with the addition of new transitions near the top of the sequence, band 2 has been observed up to 10 100.0 keV with spin $(43/2^-)$. A large number of new γ rays and levels have been assigned to this band. The absence of a measurable Doppler shift for γ rays belonging to band 1 and the deduced $B(E2)$ values for transitions from the low-energy states in band 2 suggest that both bands may be weakly deformed. Level spins, mostly adopted as tentative in the literature, have been established for all but the highest observed states in the two bands. All $\Delta I = 1$ transitions in bands 1 and 2, except the 627.8 and 676.4 keV γ rays, have been observed to have negative $\delta_{E2/M1}$ values.

The majority of the positive-parity states, previously shown as a single sequence, have been grouped into two short sequences based on their observed behavior. One of these two sequences, labeled band 3 in Fig. 1, has been explained as arising due to magnetic rotation. The properties of band 4 are however not consistent with those for magnetic rotation. The interpretations are based on the study of the level lifetimes for eight states with $E_x \geqslant 3383.2$ keV belonging to the positive-parity bands 3 and 4 from Doppler shift attenuation data. Five of these lifetime results are being reported for the first time. The decreasing trend of the reduced transition probabilities $B(M1)$ and $B(E2)$ with increasing spin, derived from the present experimental results, and the large $[B(M1)/B(E2)]$ ratios are all suggestive of the shears mechanism being responsible for the generation of angular momentum in band 3. The negative values of the multipole mixing ratios $\delta_{E2/M1}$ for the γ rays are interpreted to imply an oblate shape for the band. The experimental $B(M1)$ values and the excitation energies are also found to be consistent with the semiclassical description of the shears mechanism of Macchiavelli *et al.* The model has been used to derive the effective g factor and the strength of the effective interaction between the two blades of the shears for band 3.

ACKNOWLEDGMENTS

The authors thank the Indian National Gamma Array collaboration for setting up the array of clover detectors at the BARC-TIFR Pelletron LINAC facility at the Tata Institute of Fundamental Research (TIFR), Mumbai, India. The assistance provided by Pradipta Das and Sujib Chatterjee of the Saha Institute of Nuclear Physics in target preparation and during experiment, respectively, is wholeheartedly appreciated. The cooperation of the Pelletron operating staff is sincerely acknowledged. The authors also thank the staff of the Target Laboratory at TIFR for providing the necessary help and facilities during the experiment.

[1] C. J. Lister, M. Campbell, A. A. Chishti, W. Gelletly, L. Goettig, R. Moscrop, B. J. Varley, A. N. James, T. Morrison, H. G. Price *et al.*, Phys. Rev. Lett. **59**, 1270 (1987).

[2] E. K. Warburton, J. W. Olness, C. J. Lister, R. W. Zurmühle, and J. A. Becker, Phys. Rev. C **31**, 1184 (1985).

[3] F. Cristancho, D. R. LaFosse, C. Baktash, D. F. Winchell, B. Cederwall, J. Döring, C. J. Gross, P.-F.Hua, H.-Q. Jin, M.Korolija *et al.*, Phys. Lett. B **357**, 281 (1995).

[4] A. G. Smith, P. J. Dagnall, J. C. Lisle, D. H. Smalley, T. R. Werner, R. Chapman, C. Finck, B. Haas, M. Leddy, W. Nazarewicz *et al.*, Phys. Lett. B **355**, 32 (1995).

[5] C. Baktash, D. M. Cullen, J. D. Garrett, C. J. Gross, N. R. Johnson, W. Nazarewicz, D. G. Sarantites, J. Simpson, and T. R. Werner, Phys. Rev. Lett. **74**, 1946 (1995).

[6] D. R. LaFosse, P.-F. Hua, D. G. Sarantites, C. Baktash, Y. A. Akovali, M. Brinkman, B. Cederwall, F. Cristancho, J. Döring, C. J. Gross *et al.*, Phys. Lett. **354**, 34 (1995).

[7] P. J. Dagnall, A. G. Smith, J. C. Lisle, D. H. Smalley, R. Chapman, C. Finck, B. Haas, M. Leddy, D. Prévost, N. Rowley, and H. Savajols, Z. Phys. A **353**, 251 (1995).

[8] D. Rudolph, C. Baktash, H.-Q. Jin, C. H. Yu, I. Birriel, M. Devlin, D. R. LaFosse, I. Y. Lee, F. Lerma, A. O. Macchiavelli, J. X. Saladin, D. G. Sarantites, G. Sylvan, S. L. Tabor, D. F. Winchell, and V. Q. Wood, Phys. Lett. B **389**, 463 (1996).

[9] H.-Q. Jin, C. Baktash, M. J. Brinkman, C. J. Gross, D. G. Sarantites, I. Y. Lee, B. Cederwall, F. Cristancho, J. Döring, F. E. Durham, P.-F. Hua, G. D. Johns, M. Korolija, D. R. LaFosse, E. Landulfo, A. O. Macchiavelli, W. Rathbun, J. X. Saladin, D. W. Stracener, S. L. Tabor, and T. R. Werner, Phys. Rev. Lett. **75**, 1471 (1995).

[10] D. G. Sarantites, D. R. LaFosse, M. Devlin, F. Lerma, V. Q. Wood, J. X. Saladin, D. F. Winchell, C. Baktash, C.-H. Yu, P. Fallon, I. Y. Lee, A. O. Macchiavelli, R. W. MacLeod, A. V. Afanasjev, and I. Ragnarsson, Phys. Rev. C **57**, R1(R) (1998).

[11] H. Schnare, R. Schwengner, S. Frauendorf, F. Dönau, L. Käubler, H. Prade, A. Jungclaus, K. P. Lieb, C. Lingk, S. Skoda, J. Eberth, G. de Angelis, A. Gadea, E. Farnea, D. R. Napoli, C. A. Ur, and G. Lo Bianco, Phys. Rev. Lett. **82**, 4408 (1999).

[12] R. Schwengner, G. Rainovski, H. Schnare, A. Wagner, F. Dönau, A. Jungclaus, M. Hausmann, O. Iordanov, K. P. Lieb, D. R. Napoli, G. de Angelis, M. Axiotis, N. Marginean, F. Brandolini, and C. Rossi Alvarez, Phys. Rev. C **66**, 024310 (2002).

[13] R. Schwengner, F. Dönau, T. Servene, H. Schnare, J. Reif, G. Winter, L. Käubler, H. Prade, S. Skoda, J. Eberth *et al.*, Phys. Rev. C **65**, 044326 (2002).

[14] S. Ganguly, P. Banerjee, I. Ray, R. Kshetri, S. Bhattacharya, M. Saha-Sarkar, A. Goswami, S. Muralithar, R. P. Singh, R. Kumar, and R. K. Bhowmik, Nucl. Phys. A **768**, 43 (2006).

[15] R. Schwengner, G. Rainovski, H. Schnare, A. Wagner, S. Frauendorf, F. Dönau, A. Jungclaus, M. Hausmann, O. Yordanov, K. P. Lieb, D. R. Napoli, G. de Angelis, M. Axiotis, N. Marginean, F. Brandolini, and C. Rossi Alvarez, Phys. Rev. C **80**, 044305 (2009).

[16] S. Kumar, Naveen Kumar, S. Mandal, S. C. Pancholi, P. C. Srivastava, A. K. Jain, R. Palit, S. Saha, J. Sethi, B. S. Naidu, R. Donthi, P. K. Joshi, T. Trivedi, S. Muralithar, R. P. Singh, R. Kumar, A. Dhal, and R. K. Bhowmik, Phys. Rev. C **90**, 024315 (2014).

[17] L. Funke, J. Döring, P. Kemnitz, E. Will, G. Winter, A. Johnson, L. H. Hildingsson, and Th. Lindbald, Nucl. Phys. A **455**, 206 (1986).

[18] P. Kemnitz, J. Döring, L. Funke, G. Winter, L. H. Hildingsson, D. Jerrestam, A. Johnson, and Th. Lindbald, Nucl. Phys. A **456**, 89 (1986).

[19] S. Frauendorf, Nucl. Phys. A **677**, 115 (2000).
[20] G. Y. Zhao, G. S. Li, X. G. Wu, X. A. Liu, S. X. Wen, J. B. Lu, G. J. Yuan, and C. X. Yang, Chin. Phys. Lett. **16**, 345 (1999).
[21] S. E. Arnell, S. Sjöberg, Ö. Skeppstedt, E. Wallander, A. Nilsson, Z. P. Sawa, and G. Finnas, Z. Phys. A **289**, 89 (1978).
[22] E. K. Warburton, J. W. Olness, C. J. Lister, J. A. Becker, and S. D. Bloom, J. Phys. **G12**, 1017 (1986).
[23] R. Palit, S. Saha, J. Sethi, T. Trivedi, S. Sharma, B. S. Naidu, S. Jadhav, R. Donthi, P. V. Chavan, H. Tan, and W. Hennig, Nucl. Instrum. Methods Phys. Res., Sect. A **680**, 90 (2012).
[24] D. C. Radford, Nucl. Instrum. Methods Phys. Res., Sect. A **361**, 297 (1995).
[25] R. K. Bhowmik, INGASORT manual (private communication).
[26] E. S. Macias, W. D. Ruhter, D. C. Camp, and R. G. Lanier, Comput. Phys. Commun. **11**, 75 (1976).
[27] J. C. Wells and N. Johnson, Rep. ORNL 6689, p. 44, 1991.
[28] See Supplemental Material at http://link.aps.org/supplemental/10.1103/PhysRevC.98.034320 for Tables I–V on γ-ray relative intensities, DCO ratios, multipole mixing ratios, and level spin assignments.
[29] T. D. Johnson and W. D. Kulp, Nucl. Data Sheets **129**, 1 (2015).
[30] A. Krämer-Flecken, T. Morek, R. M. Lieder, W. Gast, G. Hebbinghaus, H. M. Jäger, and W. Urban, Nucl. Instrum. Methods Phys. Res. **275**, 333 (1989).
[31] S. Ganguly, P. Banerjee, I. Ray, R. Kshetri, R. Raut, S. Bhattacharya, M. Saha-Sarkar, A. Goswami, S. Mukhopadhyay, A. Mukherjee, G. Mukherjee, and S. K. Basu, Nucl. Phys. A **789**, 1 (2007).
[32] G. García-Bermúdez, M. A. Cardona, R. V. Ribas, A. Filevich, E. Achterberg, and L. Szybisz, Phys. Rev. C **48**, 1623 (1993).
[33] H. Grawe, K. Langanke, and G. Martínez-Pinedo, Rep. Prog. Phys. **70**, 1525 (2007).
[34] N. S. Kelsall, R. Wadsworth, S. J. Asztalos, B. Busse, C. J. Chiara, R. M. Clark, M. A. Deleplanque, R. M. Diamond, P. Fallon, D. B. Fossan, D. G. Jenkins, S. Juutinen, R. Krücken, G. J. Lane, I. Y. Lee, A. O. Macchiavelli, C. M. Parry, G. J. Schmid, J. M. Sears, J. F. Smith, F. S. Stephens, K. Vetter, and S. G. Frauendorf, Phys. Rev. C **61**, 011301(R) (1999).
[35] T. Lönnroth, S. Vajda, O. C. Kistner, and M. H. Rafailovich, Z. Phys. A **317**, 215 (1984).
[36] A. W. Mountford, T. Vass, G. Kumbartzki, L. A. Bernstein, N. Benczer-Koller, R. Tanczyn, C. J. Lister, P. Chowdhury, and S. J. Freeman, Phys. Rev. C **51**, 513 (1995).
[37] A. O. Macchiavelli, R. M. Clark, P. Fallon, M. A. Deleplanque, R. M. Diamond, R. Krücken, I. Y. Lee, F. S. Stephens, S. Asztalos, and K. Vetter, Phys. Rev. C **57**, R1073(R) (1998).
[38] A. Görgen, N. Nenoff, H. Hübel, G. Baldsiefen, J. A. Becker, A. P. Byrne, S. Chmel, R. M. Clark, M. A. Deleplanque, R. M. Diamond, P. Fallon, K. Hauschild, I. M. Hibbert, W. Korten, R. Krücken, I. Y. Lee, A. O. Macchiavelli, E. S. Paul, U. J. van Severen, F. S. Stephens, K. Vetter, R. Wadsworth, A. N. Wilson, and J. N. Wilson, Nucl. Phys. A **683**, 108 (2001).
[39] R. M. Clark, S. J. Asztalos, B. Busse, C. J. Chiara, M. Cromaz, M. A. Deleplanque, R. M. Diamond, P. Fallon, D. B. Fossan, D. G. Jenkins, S. Juutinen, N. Kelsall, R. Krücken, G. J. Lane, I. Y. Lee, A. O. Macchiavelli, R. W. MacLeod, G. Schmid, J. M. Sears, J. F. Smith, F. S. Stephens, K. Vetter, R. Wadsworth, and S. Frauendorf, Phys. Rev. Lett. **82**, 3220 (1999).
[40] Santosh Roy, Pradip Datta, S. Pal, S. Chattopadhyay, S. Bhattacharya, A. Goswami, H. C. Jain, P. K. Joshi, R. K. Bhowmik, R. Kumar, S. Muralithar, R. P. Singh, N. Madhavan, and P. V. Madhusudhana Rao, Phys. Rev. C **81**, 054311 (2010).
[41] P. Banerjee, S. Ganguly, M. K. Pradhan, H. P. Sharma, S. Muralithar, R. P. Singh, and R. K. Bhowmik, Phys. Rev. C **83**, 024316 (2011).